ACS OMEGA
http://pubs.acs.org/journal/acsodf
Article

Impact of Bonding Temperature on Microstructure, Mechanical, and Fracture Behaviors of TLP Bonded Joints of Al2219 with a Cu Interlayer

Manjunath Vatnalmath, Virupaxi Auradi,* Varun Kumar M J, Bharath Vedashantha Murthy, Madeva Nagaral,* A. Anbarasa Pandian, Saiful Islam, Mohammad Shahiq Khan, Chandrashekar Anjinappa, and Abdul Razak*

Cite This: ACS Omega 2023, 8, 26332−26339

Read Online

ACCESS | Metrics & More | Article Recommendations

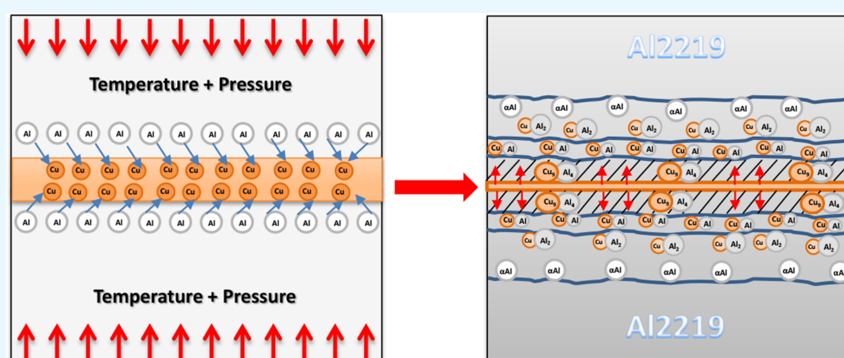

ABSTRACT: The present study aims at producing transient liquid phase (TLP) bonded Al2219 joints with pure Cu (copper) as an interlayer. The TLP bonding is carried out at the bonding temperatures in the range of 480 to 520 °C while keeping the bonding pressure (2 MPa) and time (30 min.) constant. Reaction layers are formed at the Al-Cu interface with a significant increase in diffusion depth with the increase in the bonding temperature. The microstructural investigations are carried out using scanning electron microscopy and energy-dispersive spectroscopy. X-ray diffraction study confirms the formation of $CuAl_2$, CuAl, and Cu_9Al_4 intermetallic compounds across the interface of the bonded specimens. An increase in microhardness is observed across the bonding zone with the increase in the bonding temperature, and a maximum hardness value of 723 Hv is obtained on the diffusion zone of the specimen bonded at 520 °C. Furthermore, the fractography study of the bonded specimens is carried out, and a maximum shear strength of 18.75 MPa is observed on the joints produced at 520 °C.

1. INTRODUCTION

Several industries utilize aluminum (Al) alloys as component materials, including aircraft bodies, packaging of electric modules, electronic technology, automobile body structures, wind energy management, and solar energy production. Although composites have become increasingly prevalent, Al alloys remain a fundamental material for structural applications owing to their lightweight, workability, and low cost, and significant improvements have been made, especially for 2XXX, 7XXX, and Al-Li alloys.[1,2] Al-Cu alloy 2219 is used widely in the aerospace industry, primarily in the construction of fuel tanks, due to its low density, high strength, stress corrosion resistance, good weldability, and admirable cryogenic properties.[3,4] Joining aluminum alloys with other metal alloys has gained more attention in the field of aerospace because of the advantages of hybrid joints in terms of their enhanced mechanical properties.

Furthermore, there are many different applications, such as linking battery tab to bus bars, electrical connectors, transformer foil conductors, condenser and capacitor foil windings, heat exchanger tubing, refrigeration tubes, and tube covers, frequently using aluminum and copper dissimilar joints. Hybrid joints of Al and Cu are eventually gaining importance due to their high conductivity and light weight properties as copper has high diffusivity and allows for high heat flux. However, joining aluminum alloys to other metal alloys using

Received: April 25, 2023
Accepted: June 30, 2023
Published: July 17, 2023

ACS Publications
© 2023 The Authors. Published by American Chemical Society

conventional fusion welding is not recommended due to the formation of weld flaws and brittle intermetallics at the interface. Advanced welding techniques such as TIG and MIG generate welding defects such as porosity, cracks, and incomplete penetration, and friction stir welding is a complex process where identification of the defects produced at the interface is not simple.[5−10]

Recently, solid-state diffusion bonding (SSDB) has been developed to fabricate similar and dissimilar joints with excellent mechanical properties. The main principle of SSDB is based on the interatomic diffusion across the interface of the two metals or metal alloys. SSDB is usually carried out in the temperature range of 50−80% of the absolute melting point of the base metal.[11,12] Generally, three parameters that influence the diffusion bonding process are temperature, pressure, and time.[13,14] High pressure brings the bonding surfaces into close contact, and elevated temperature produces a high degree of molecular activity, resulting in grain formation across the interface. Since the process is not instinctive, an optimum bonding time is required to produce strong joints. However, many combinations of these three parameters can be used to produce strong joints.[15]

The incorporation of a suitable interlayer between the two nominally flat metal surfaces would produce a joint with higher mechanical properties than the base metal. This method is mainly termed transient liquid phase (TLP) bonding and alternatively as diffusion brazing, which is widely used in joining heterogeneous materials. TLP bonding can be carried out either by forming eutectics at the interface using an interlayer whose melting point is greater than the bonding temperature or by employing an interlayer whose melting point is within the bonding temperature range. Interlayers are used in diffusion bonding to reduce chemical heterogeneity and thermodynamic instability in the transition zone of the joint, as well as to prevent or restrict the effects of temperature deformation considerably while joining dissimilar metals. The interdiffusion that occurs between the interlayer and the base metal makes the TLP bonding technique effective for joining dissimilar metals with a large difference in thermal properties.[16−24]

A study on joining similar alloys conducted by Liu et al.[25] reported the feasibility and formation mechanism of air diffusion bonded joints of Al-Mg-Li alloys with an electrodeposited coating of nano-Cu as an interlayer. However, diffusion bonding is always preferred to be carried out in a vacuum or inert atmosphere to completely inhibit the formation of oxides as aluminum surfaces are always prone to strong oxide formation. Nadermanesh et al.[26] investigated the diffusion bonding of Al alloys 7075, 5083, and 6061 to magnesium alloy using 20 μm copper as an interlayer, and it was revealed that increasing the temperature induces the formation of thicker interface layers, indicating intermetallic compounds (IMCs) such as $CuAl_2$ and Cu_9Al_4 at the Al-Cu interface. Saleh[27] found only $CuAl_2$ phase on diffusion-bonded joints of Al2014 with copper powder as an interlayer. An SSDB study on aluminum alloy and pure copper conducted by Bedjaoui et al.[28] revealed five major IMCs such as $CuAl_2$, CuAl, Cu_4Al_3, Cu_3Al_2, and Cu_9Al_4 at the interface of the bonded joints. However, many studies have reported difficulty in finding all major IMCs due to the low volume fraction of some phases and which are difficult to investigate viz. X-ray diffraction (XRD), as the bonding temperature, pressure, and holding time affect the formation of IMCs at the interface.

Although several studies on the solid-state welding of various aluminum alloys with copper have been performed, no recent study on the diffusion bonding of Al2219 and Cu has been found. In the present study, the TLP bonded joints of Al2219 with copper as the interlayer are evaluated for interfacial microstructure, microhardness across the bonding interface, and shear strength of the joints.

2. EXPERIMENTAL PROCEDURE

The base metal Al2219 (Cu-6.48, Si-0.49, Fe-0.23, Mn-0.32, Mg-0.01, Zr-0.2, V-0.08, Ti-0.06, Zn-0.18, Al-Bal, wt %) specimens are prepared to a dimension of 50 × 50 × 5 mm^3 using wire cut electrical discharge machining (EDM), and then the faying surfaces are polished using different SiC grits (220−1200). Polished specimens are chemically washed with 6% NaOH and 30% HNO_3 and then ultrasonically cleaned in an acetone bath and dried using hot air. A copper (99.9% pure) foil of 50 μm, prior cleaned with ethanol, is placed between the two faying surfaces of Al2219. The stacked arrangement is then immediately placed in the bonding furnace for the diffusion bonding process. The diffusion bonding system used in the current study is schematically shown in Figure 1.

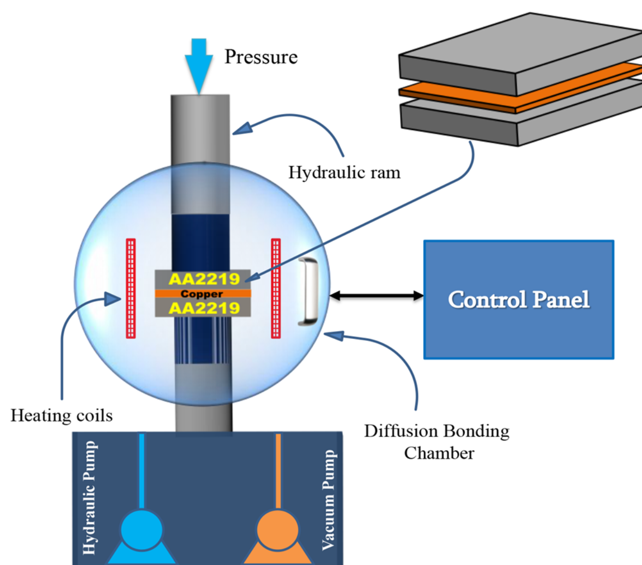

Figure 1. Schematic representation of the diffusion bonding furnace.

Diffusion bonding is performed at the bonding temperatures of 480, 500, and 520 °C, keeping pressure (2 MPa) and time (30 min) constant. After the bonding process, specimens are furnace cooled without releasing the bonding pressure to avoid thermal shocks, and then diffusion bonded specimens are cut perpendicularly to the joint section with the help of wire cut EDM for microstructural analysis. The resulting cut samples are then grounded using different SiC grits (320−2000) and finally polished with diamond paste (1 μ). The polished, cut samples are then etched using Keller's reagent just before the microstructural analysis. Scanning electron microscopy (SEM, TESCAN-VEGA3 LMU) is used to analyze the microstructure of the base metal and interface. The variations in elemental composition across joint sections are examined using energy-dispersive spectroscopy (EDS), and XRD is employed mainly to investigate the intermetallics formed across the interface of the bonded joints. The hardness measurements across the joint section are tested using a Vickers microhardness test rig

https://doi.org/10.1021/acsomega.3c02838
ACS Omega 2023, 8, 26332−26339

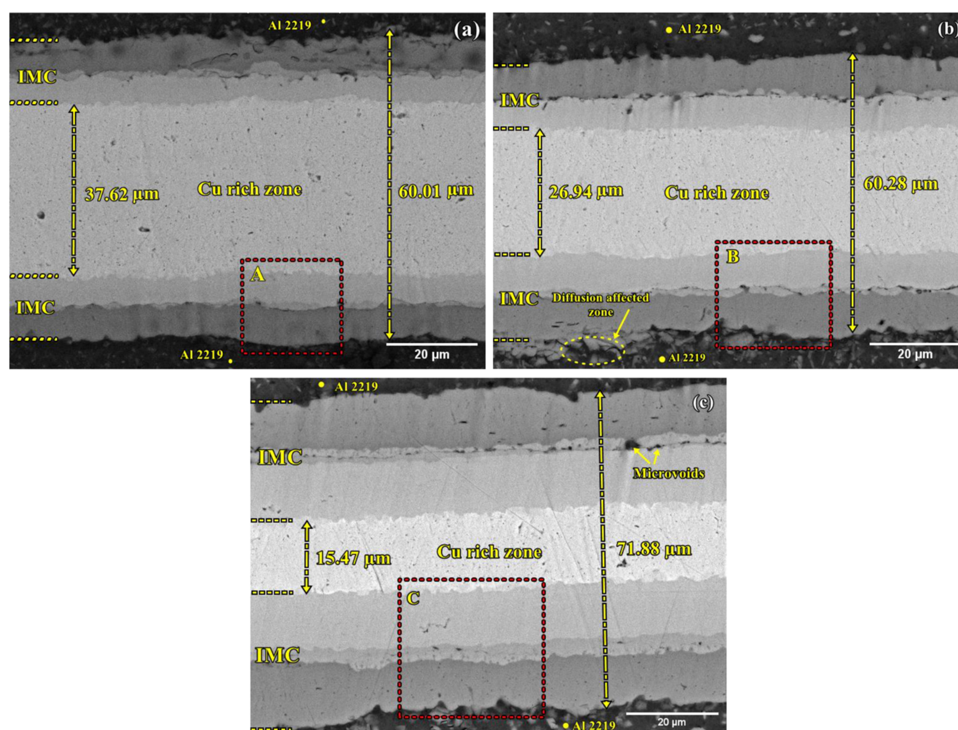

Figure 2. BSE images of diffusion bonded specimens at (a) 480 °C, (b) 500 °C, and (c) 520 °C.

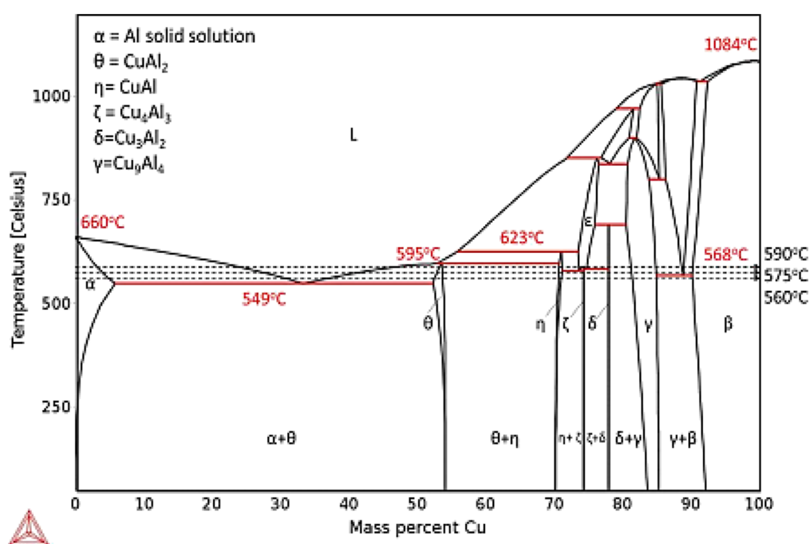

Figure 3. Al-Cu binary phase diagram.[30]

(MICRO-MACH) with an indentation load of 50 g and a dwell period of 10 s. Joint strength is evaluated by shear test (BISS-25 kN) with a loading rate of 1 mm/min at room temperature conditions.

3. RESULTS AND DISCUSSION

3.1. Microstructure. Initially, an SSDB instigates between the aluminum and copper surfaces as the melting point of the copper interlayer is higher than that of Al2219.[24] Then, at an adequate temperature, and well within the melting temperature of aluminum, a eutectic reaction between Al2219 and copper occurs, in which Cu-rich atoms diffuse into aluminum.[29] Figure 2a−c shows the backscatter electron (BSE) images of the specimens bonded at 480, 500, and 520 °C. A diffusion zone of

Table 1. Composition Variation of Elements Confirmed by EDS

EDS points (Figure 4)	Al at%	Cu at%	probable phase
1	35.82	64.18	Cu_9Al_4
2	48.56	51.44	$CuAl + Cu_4Al_3$
3	74.28	25.72	α-Al + $CuAl_2$
4	43.99	56.01	$Cu_4Al_3 + Cu_3Al_2$
5	57.98	42.02	$CuAl_2 + CuAl$
6	71.80	28.20	α-Al + $CuAl_2$
7	45.42	54.58	$CuAl + Cu_4Al_3$
8	56.11	43.89	$CuAl_2 + CuAl$
9	72.34	27.66	α-Al + $CuAl_2$

https://doi.org/10.1021/acsomega.3c02838
ACS Omega 2023, 8, 26332−26339

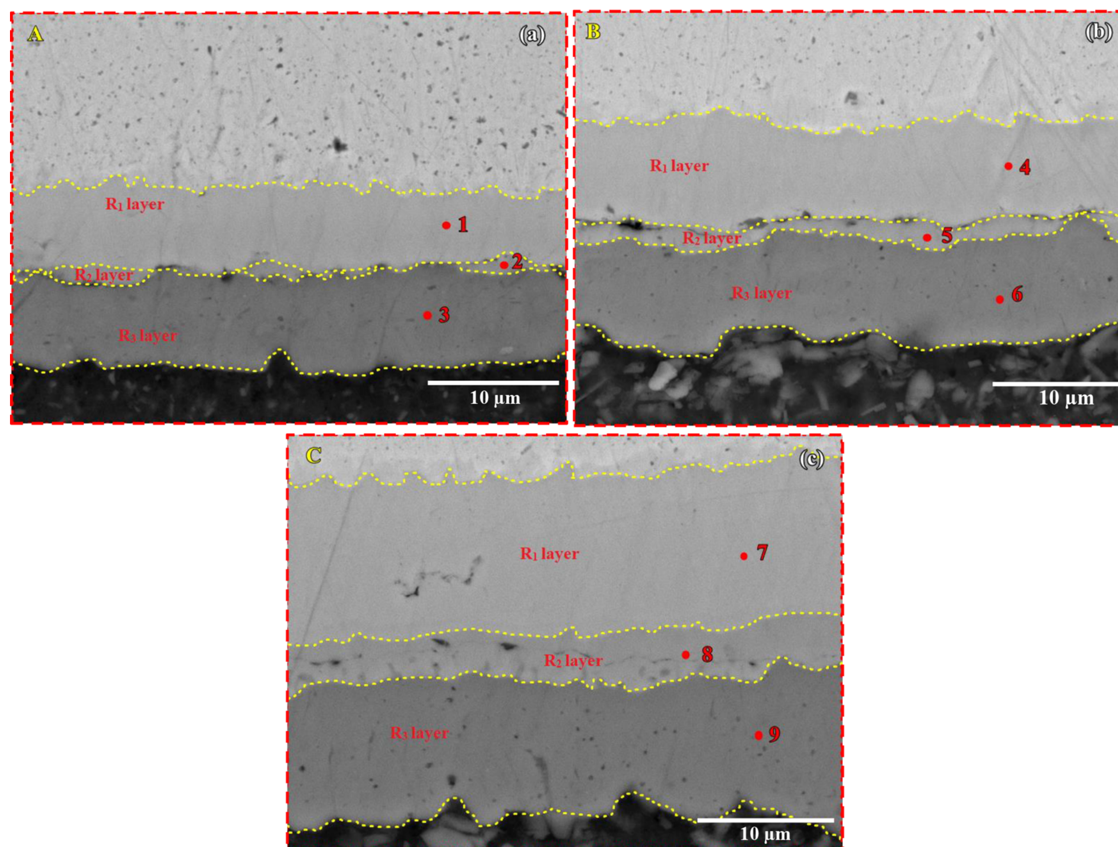

Figure 4. Magnified view of areas A, B, and C marked in Figure 2a−c.

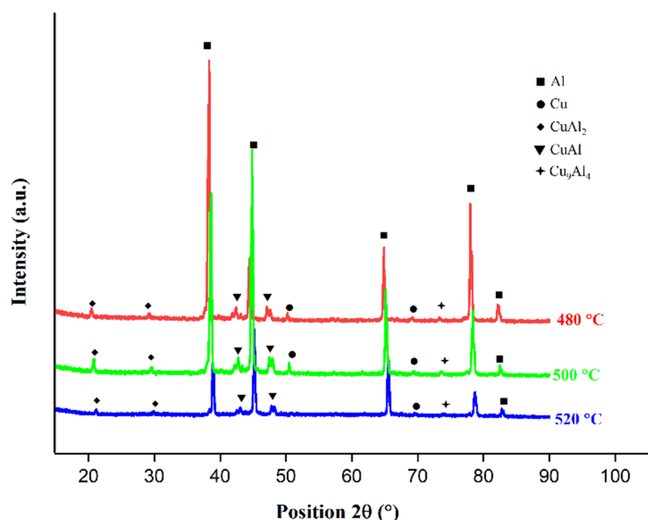

Figure 5. XRD pattern for the specimens bonded at 480, 500, and 520 °C.

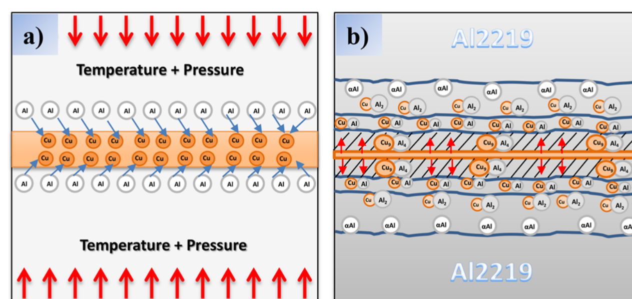

Figure 6. TLP bonding formation mechanism: (a) TLP bonding process. (b) IMC formation.

thickness 60.01 μm is observed at the bonding temperature of 480 °C, with a wider Cu-rich zone of thickness 37.62 μm (Figure 2a). When the bonding temperature is increased to 500 °C, the diffusion zone increased to a thickness of 60.28 μm, whereas the Cu-rich zone reduced to a thickness of 26.94 μm (Figure 2b).

However, when the bonding temperature is further increased to 520 °C, a thicker diffusion zone of 71.88 μm is formed, with wider IMC layers toward Al2219, and the Cu-rich zone is reduced to a thickness of 15.47 μm (Figure 2c). The thickness of the bonded zone on all specimens is measured in 20 different areas and then averaged.

The increase in the thickness of the diffusion zone is mainly attributed to the improved interdiffusion with the increase in the bonding temperature, and meanwhile, the thickness of the copper interlayer is effectively reduced. The binary phase diagram[30] of Al-Cu shown in Figure 3 predicts the formation of IMCs like $CuAl_2$ (θ), CuAl (η), Cu_4Al_3 (ζ), Cu_3Al_2 (δ), and Cu_9Al_4 (γ). Lee and Kwon[31] reported the difficulty in finding Cu_3Al_2 (ζ) and Cu_3Al_2 (δ) phases, anticipating that the short bonding time generates thin, unclear reaction layers that may have intermixed with different IMCs.

All bonded specimens exhibit three IMC reaction layers and are depicted as R_1, R_2, and R_3 having different concentrations of Al and Cu elements. The EDS analysis is carried out to investigate the composition variation of each element at different IMC reaction layers (Table 1). Figure 4a−c shows the

https://doi.org/10.1021/acsomega.3c02838
ACS Omega 2023, 8, 26332−26339

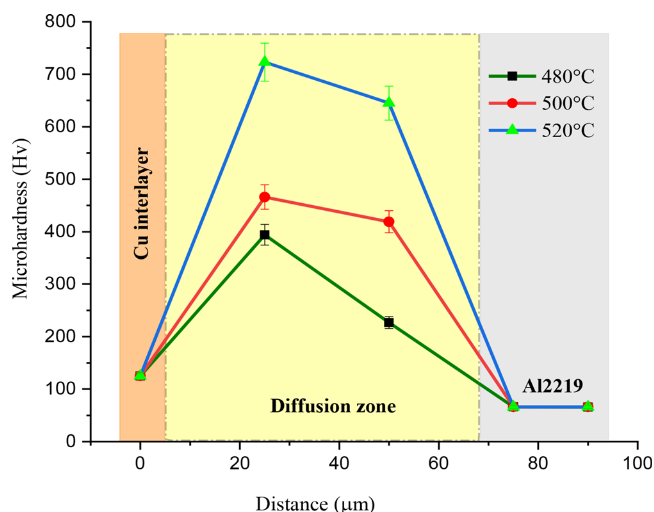

Figure 7. Microhardness profile across the TLP bonded joints.

magnified view of the diffusion zones of the TLP bonded specimens as marked in Figure 2a−c.

3.2. IMC at the Interface of the TLP Joints. The IMC reaction layers formed on the bonded sections are depicted as R_1, R_2, and R_3. The R_3 layer (Figure 4a) appears dark gray, with 55.08 wt % of aluminum and 44.92 wt % of copper, indicating the presence of the α-Al + $CuAl_2$ phase, and the R_1 layer (Figure 4a) appears light gray, with 80.84% wt % of copper and 19.16 wt % of aluminum, which predominate the presence of Cu_9Al_4. However, in the specimen bonded at 500 °C, the R_2 layer (Figure 4b) is observed as a continuous band compared to that of the section bonded at 480 °C, and it has 63.05 wt % of copper and 36.95% of aluminum, whereas the R_1 layer (Figure 4b) has 74.99 wt % of copper and 25.01% of aluminum, speculating the phase CuAl + Cu_4Al_3. When the bonding temperature is further increased to 520 °C, a continuous and thick R2 layer (Figure 4c) of width 3.57 μm is formed. It has 64.82 wt % of copper and 35.18 wt % of aluminum, predicting the $CuAl_2$ + CuAl phase in it. Figure 5 shows the XRD patterns of the TLP bonded specimens for further confirmation of IMC, which are formed at the interface of Al-Cu. Only three phases, $CuAl_2$ (θ), CuAl (η), and Cu_9Al_4 (γ), are observed, whereas Cu_4Al_3 (ζ) and Cu_3Al_2 (δ) are not found for the current TLP bonding conditions.

3.3. Formation Mechanism of TLP Joints. Initially, the $CuAl_2$ phase is observed at the interface between aluminum and copper as the maximum solid solubility of Cu in Al is 2.48 at%, whereas that of Al in Cu is 19.7 at%. Hence, Al atoms diffuse into the copper readily, leaving vacancies on the aluminum side, and the Cu-rich atoms, which have lower diffusivity, occupy these vacancies created on the Al side.[32−36]

The combined effect of temperature and pressure makes Al diffuse into Cu early and forms α-Al and $CuAl_2$ at the bonding interface. During diffusion bonding, Cu diffuses into aluminum at low ratios to a longer distance, whereas Al diffuses into copper at a faster rate but to a shorter distance. The main cause, for this reason, is the smaller atomic diameter of the Cu atoms compared to that of Al atoms. The earlier formation of IMC in copper would also be due to the short diffusion depth of Al in copper.[37] When an adequate bonding temperature has reached, the Cu-rich atoms start to diffuse slowly into Al and form Cu_9Al_4 phase near the copper interlayer which is schematically represented in Figure 6b.

3.4. Microhardness. Figure 7 shows how the microhardness profile for the TLP-bonded joints formed at 480, 500, and 520 °C. The hardness of the base metal, the diffusion zone, and the copper interlayer is found by taking 10 readings at different indent sites and taking the average of them. A maximum hardness of 66 Hv is observed on Al2219 base metal, whereas on the copper interlayer, it is 125 Hv.

At the interface of the bonded specimens, it is observed that the hardness is increased with an increase in the bonding temperature. Maximum hardness of 394 and 466 Hv is observed at the interface for the specimens bonded at 480 and 500 °C, respectively, whereas the specimen bonded at 520 °C exhibits a maximum hardness of 723 Hv at the bonding interface. Hence, it elucidates the formation of brittle IMC near the Cu interlayer. However, the hardness has been decreased when it is tested away from the Cu interlayer and near the Al2219 base metal.

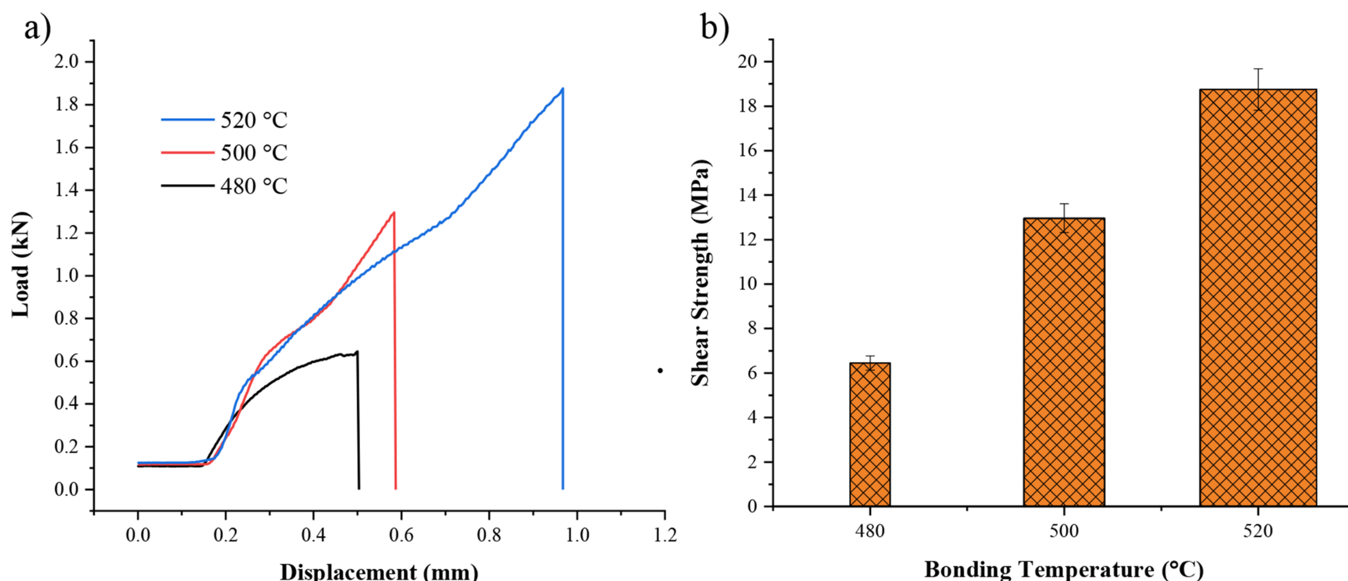

Figure 8. Shear test results. (a) Load−displacement profile. (b) Shear strength of the TLP joints as a function of temperature.

https://doi.org/10.1021/acsomega.3c02838
ACS Omega 2023, 8, 26332−26339

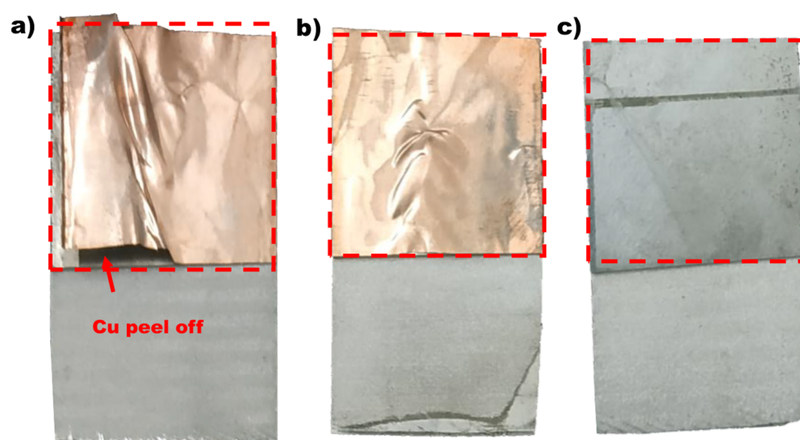

Figure 9. Peel-off type fracture at the bonding interface. (a) 480 °C, (b) 500 °C, and (c) 520 °C ("Photograph courtesy of 'Manjunath Vatnalmath'. Copyright 2022.")

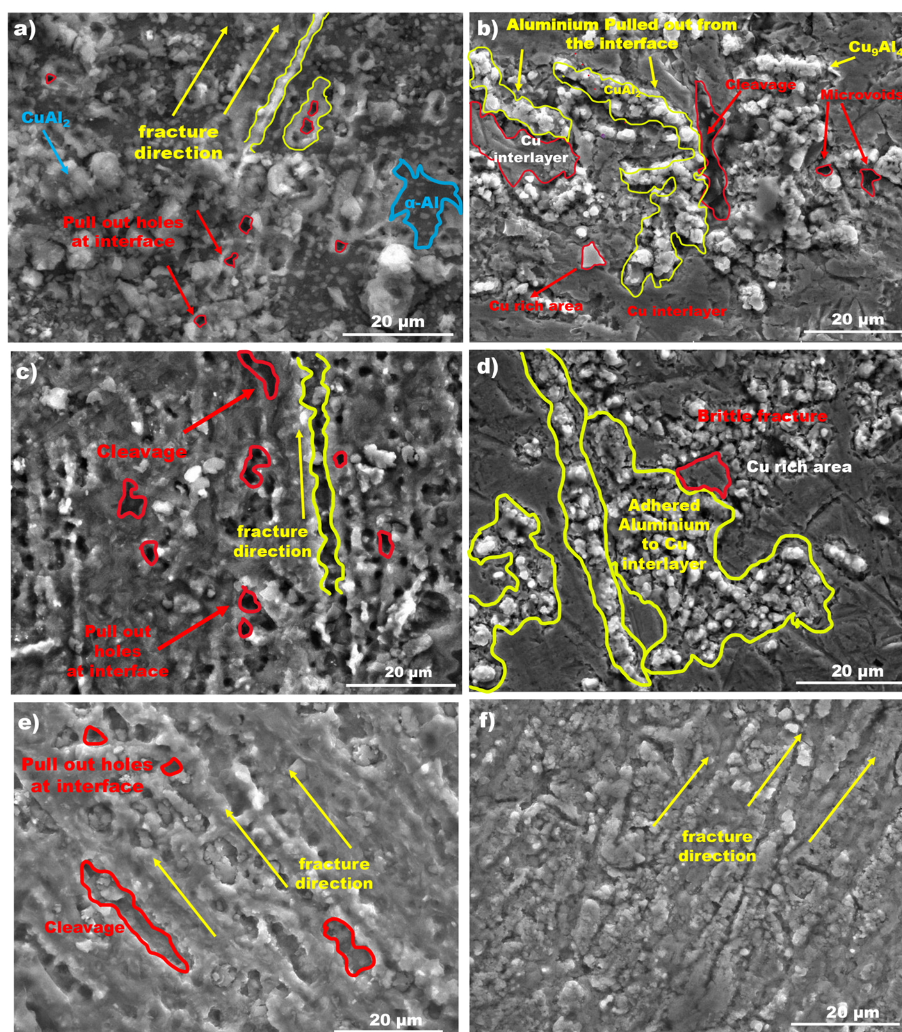

Figure 10. SEM images of fractured surfaces of specimens bonded at 480 °C (a,b), 500 °C (c,d), and 520 °C (e,f).

3.5. Shear Strength of TLP Bonded Joints. Figure 8a shows the load−displacement profile, and Figure 8b shows the shear strength of the TLP bonded joints as a function of temperature. The shear test of the TLP bonded joints is performed at room temperature, and it is observed that all the bonded specimens failed at the joint interface. A peel-off type fracture is observed for the specimens bonded at 480 and 500 °C, in which the copper interlayer is pulled out from the bonding interface at the time of shear failure, as shown in Figure 9a,b. However, at 500 °C (Figure 9c), copper interlayer has been completely bonded to both Al base metals, and the copper interlayer peeling off is not observed. Furthermore, it is

https://doi.org/10.1021/acsomega.3c02838
ACS Omega 2023, 8, 26332−26339

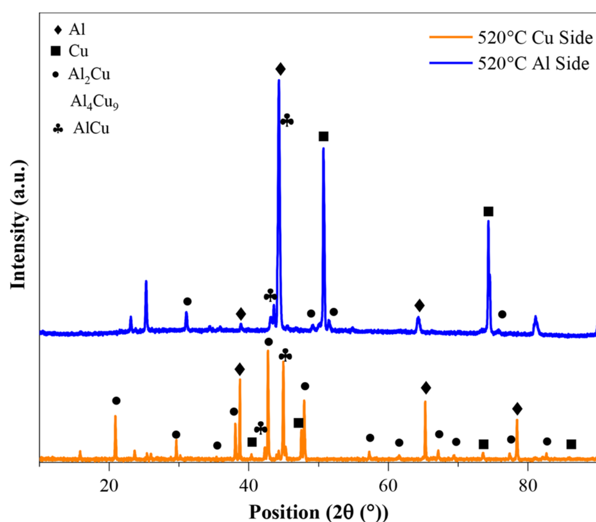

Figure 11. XRD pattern for the fractured specimen bonded at 520 °C.

evident from the results that the shear strength increases with an increase in the bonding temperature. A shear strength of 6.45 and 12.96 MPa is obtained for the specimens bonded at 480 and 500 °C, respectively.

There is an increase in the shear strength to 18.75 MPa for the specimen bonded at 520 °C. The increase in shear strength is mainly attributed to the microstructure of the bonding interface as the higher temperature reduced the formation of microvoids and delamination between the IMC reaction layers.

3.6. Fractography. Figure 10 shows the SEM images of the fractured surfaces of the TLP bonded specimens which are examined to know the impact of the bonding temperature on the fracture mechanism. A brittle type of fracture can be seen on all bonded surfaces as all TLP bonded specimens failed at the bonding interface. Figure 10a−d shows the fractured surfaces of the specimens bonded at 480 and 500 °C, where a large number of pull-out holes on the Al side and adhered Al on the Cu side can be observed. Plastic deformation of aluminum is not observed on the fractured surfaces, and this indicates a brittle failure at these bonding temperature conditions. This type of fracture also would be affected by the delamination produced between the IMC reaction layers. However, when the bonding temperature increased to 520 °C (Figure 10e,f), delamination of Al materials and voids are not detected on both the fractured surfaces, and a good bonding strength of 18.75 MPa is noted compared to the specimens bonded at 480 and 500 °C.

Figure 11 shows the XRD pattern for the fractured surfaces of the Al and Cu sides for the specimen bonded at 520 °C. The peaks illustrate the formation of Cu_9Al_4, $CuAl_2$, and CuAl along with pure Al and Cu. Hence, the XRD peaks of fractured surfaces support the IMC formation mechanism at the interface.

4. CONCLUSIONS

TLP diffusion bonded joints of Al2219 with a copper interlayer are successfully produced, and the intermetallic compounds formed across the diffusion joints are investigated over the temperature range of 480−520 °C.

- The bonded specimens exhibit three IMC reaction layers at the bond interface of Al−Cu, and in addition, it is observed that the interface thickness of the bonding zone increased with an increase in the bonding temperature.
- The diffusion thickness of 60.01, 60.28, and 71.88 μm is obtained for the bonding temperatures of 480, 500, and 520 °C, respectively.
- In the present study, only three intermetallic phases, $CuAl_2$ (θ), CuAl (η), and Cu_9Al_4 (γ), are found among the five major phases.
- The hardness at the interface of the bonded sections increased with an increase in the bonding temperature, and a maximum hardness of 723 Hv is found on the diffusion zone of the specimen bonded at 520 °C.
- An increase in shear strength is observed with the increase in the bonding temperature, and a maximum shear strength of 18.75 MPa is observed for the specimen bonded at 520 °C.

■ AUTHOR INFORMATION

Corresponding Authors

Virupaxi Auradi − *Department of Mechanical Engineering, Siddaganga Institute of Technology, Visvesvaraya Technological University, Tumakuru, Karnataka 572103, India;* orcid.org/0000-0001-6549-6340; Email: vsauradi@gmail.com

Madeva Nagaral − *Aircraft Research and Design Centre, HAL, Bangalore, Karnataka 560037, India;* orcid.org/0000-0002-8248-7603; Email: madev.nagaral@gmail.com

Abdul Razak − *Department of Mechanical Engineering, P. A. College of Engineering (Affiliated to Visvesvaraya Technological University, Belagavi), Mangaluru 574153, India;* orcid.org/0000-0001-7985-2502; Email: arkmech9@gmail.com

Authors

Manjunath Vatnalmath − *Department of Mechanical Engineering, Siddaganga Institute of Technology, Visvesvaraya Technological University, Tumakuru, Karnataka 572103, India;* orcid.org/0000-0003-3138-9453

Varun Kumar M J − *Department of Mechanical Engineering, RNS Institute of Technology, Visvesvaraya Technological University, Bangalore, Karnataka 560098, India*

Bharath Vedashantha Murthy − *Department of Mechanical Engineering, RNS Institute of Technology, Visvesvaraya Technological University, Bangalore, Karnataka 560098, India;* orcid.org/0000-0001-6765-4728

A. Anbarasa Pandian − *Department of Computer Science and Engineering, Panimalar Engineering College, Chennai 602103, India*

Saiful Islam − *Civil Engineering Department, College of Engineering, King Khalid University, Abha 61421, Saudi Arabia*

Mohammad Shahiq Khan − *Civil Engineering Department, College of Engineering & IT, Onaizah Colleges, Al Qassim University, Buraidah, Al-qassim 52571, Saudi Arabia*

Chandrashekar Anjinappa − *Department of Robotics and Artificial Intelligence, Bangalore Institute of Technology, Visvesvaraya Technological University, Bengaluru, Karnataka 560004, India*

Complete contact information is available at:
https://pubs.acs.org/10.1021/acsomega.3c02838

Notes

The authors declare no competing financial interest.

■ ACKNOWLEDGMENTS

The authors extend their appreciation to the Deanship of Scientific Research at King Khalid University for funding this work through large group Research Project under grant number RGP2/556/44.

■ REFERENCES

(1) Varshney, D.; Kumar, K. Application and use of different aluminium alloys with respect to workability, strength and welding parameter optimization. *Ain Shams Eng. J.* **2021**, *12*, 1143−1152.

(2) Gloria, A.; Montanari, R.; Richetta, M.; Varone, A. Alloys for aeronautic applications: state of the art and perspectives. *Metals* **2019**, *9*, 662.

(3) Zhao, Y.; Qi, N.; Li, Y.; Gu, Y.; Zhan, X. Research on the cryogenic axial tensile fracture mechanism for 2219 aluminum alloy T-joint by dual laser-beam bilateral synchronous welding. *Opt. Laser Technol.* **2022**, *148*, No. 107706.

(4) Wan, Z.; Zhao, Y.; Wang, Q.; Zhao, T.; Li, Q.; Shan, J.; Wang, G. Microstructure-based modeling of the PMZ mechanical properties in 2219-T8 aluminum alloy TIG welding joint. *Mater. Des.* **2022**, *223*, No. 111133.

(5) Akca, E.; Gürsel, A. The importance of interlayers in diffusion welding-A review. *Period. Eng. Nat. Sci.* **2016**, *3*, 12−16.

(6) Rudrapati, R. *Recent advances in joining of aluminum alloys by using friction stir welding: Mass Production Processes*; IntechOpen, 2020.

(7) Chandrashekar, A.; Chaluvaraju, B. V.; Afzal, A.; Denis, A.; Kaladgi, A. R.; Alamri, S.; Ahamed Saleel, C.; Tirth, V. Mechanical and Corrosion Studies of Friction Stir Welded Nano Al2O3 Reinforced Al-Mg Matrix Composites: RSM-ANN Modelling Approach. *Symmetry* **2021**, *13*, 537.

(8) Kah, P.; Rajan, R.; Martikainen, J.; Suoranta, R. Investigation of weld defects in friction-stir welding and fusion welding of aluminium alloys. *Int. J. Mech. Mater. Eng.* **2015**, *10*, 26.

(9) Teng, Q.; Li, X.; Wei, Q. Diffusion bonding of Al 6061 and Cu by hot isostatic pressing. *J. Wuhan Univ. Technol. Mater. Sci. Ed.* **2020**, *35*, 183−191.

(10) Isa, M. S. M.; Moghadasi, K.; Ariffin, M. A.; Raja, S.; Bin Muhamad, M. R.; Yusof, F.; Jamaludin, M. F.; Bin Yusoff, N.; Bin Ab Karim, M. S. Recent research progress in friction stir welding of aluminium and copper dissimilar joint: a review. *J. Mater. Res. Technol.* **2021**, *15*, 2735−2780.

(11) Demeneghi, G.; Rodgers, K.; Su, C. H.; Medders, W. M.; Gorti, S.; Wilkerson, R. Root cause analysis of premature simulated life cycle failure of friction stir welded aluminum 2219. *Eng. Fail. Anal.* **2022**, *134*, No. 106059.

(12) Baghdadi, L.; Boumerzoug, Z.; Brisset, F.; Solas, D.; Baudin, T. Solid-state diffusion bonding of X70 steel to duplex stainless steel. *Acta Metall. Slovaca* **2022**, *28*, 106−112.

(13) Latouche, T.; Cailler, M.; Sander, B.; Marya, S. K. Diffusion bonding of A2017 aluminium alloy. *Weld. Int.* **1990**, *4*, 964−969.

(14) Zhu, F.; Li, X.; Peng, H.; Zhao, H.; Xiong, L.; Chen, J. Analytical approaches to describe diffusion bonding of similar and dissimilar materials. *Sci. Technol. Weld. Join.* **2020**, *25*, 661−668.

(15) Barta, I. M. Low temperature diffusion bonding of aluminum alloys. *Weld. J.* **1964**, *43*, 241−247.

(16) Zhang, J.; Yu, L.; Liu, Y.; Liu, C.; Ma, Z.; Li, H.; Long, D. Stable bonding of W and ODS steel fabricated by TLP diffusion technology through inserting a novel composite interlayer Zr/Cu. *J. Mater. Process. Technol.* **2022**, *299*, No. 117341.

(17) Alhazaa, A.; Haneklaus, N. Diffusion Bonding and Transient Liquid Phase (TLP) Bonding of Type 304 and 316 Austenitic Stainless Steel—A Review of Similar and Dissimilar Material Joints. *Metals* **2020**, *10*, 613.

(18) Stosz, M.; Narayanasamy, S.; Graule, T.; Kata, D.; Blugan, G. Low Temperature Transient Liquid Phase Bonding of Alumina Ceramics with the Bi2O3-ZnO Interlayer. *Materials (Basel)* **2022**, *15*, 6940.

(19) Binesh, B.; Aghaie-Khafri, M.; Fayegh, A. Processing of IN718/Ti−6Al−4V bimetallic joint using transient liquid phase bonding: effect of bonding temperature on the microstructure and mechanical properties. *Philos. Mag.* **2022**, *102*, 745−772.

(20) Varmazyar, J.; Khodaei, M. Diffusion bonding of aluminum-magnesium using cold rolled copper interlayer. *J. Alloys Compd.* **2019**, *773*, 838−843.

(21) Zeer, G. M.; Zelenkova, E. G.; Koroleva, Y. P.; Mikheev, A. A.; Prokopy'ev, S. V. Diffusion bonding through interlayers. *Weld. Int.* **2013**, *27*, 638−643.

(22) Cai, X. Q.; Wang, Y.; Yang, Z. W.; Wang, D. P.; Liu, Y. C. Transient liquid phase (TLP) bonding of Ti2AlNb alloy using Ti/Ni interlayer: microstructure characterization and mechanical properties. *J. Alloys Compd.* **2016**, *679*, 9−17.

(23) Chen, M.; Jiang, B.; Ding, R.; Liu, Y.; Yu, L.; Wang, Z.; Liu, Y.; Liu, Y. Microstructure evolution and tensile behaviors of dissimilar TLP joint of austenitic steel and high-Cr ferritic steel. *Mater. Sci. Eng. A.* **2023**, *870*, No. 144818.

(24) Zhang, J.; Huang, Y.; Liu, Y.; Wang, Z. Direct diffusion bonding of immiscible tungsten and copper at temperature close to Copper's melting point. *Mater. Des.* **2018**, *137*, 473−480.

(25) Liu, Y.; Wang, G.; Chen, Y.; Kang, Q.; Luo, S.; Li, Z.; Xu, X.; Liu, Q.; Sui, X. Air atmosphere diffusion bonding of Al−Mg−Li alloy using Cu nano-coating interlayer: Microstructural characterization and formation mechanisms. *Mater. Des.* **2022**, *215*, No. 110431.

(26) Nadermanesh, N.; Azizi, A.; Manafi, S. Mechanical and microstructure property evaluation of diffusion bonding of 5083, 6061 and 7075 aluminium to AZ31 magnesium using Cu interlayer. *Proc. Inst. Mech. Eng. B J. Eng. Manuf.* **2021**, *235*, 2118−2131.

(27) Saleh, A. A. Microstructure and strength of diffusion bonded 2014 AA alloys using copper interlayer. *Open J. Appl. Sci.* **2019**, *9*, 342−353.

(28) Bedjaoui, W.; Boumerzoug, Z.; Delaunois, F. Solid-State Diffusion Welding of Commercial Aluminum Alloy with Pure Copper. *Int. J. Automot. Mech. Eng.* **2022**, *19*, 9734−9746.

(29) AlHazaa, A.; Khan, T. I.; Haq, I. Transient liquid phase (TLP) bonding of Al7075 to Ti−6Al−4V alloy. *Mater. Charact.* **2010**, *61*, 312−317.

(30) Zaheri, A.; Farahani, M.; Sadeghi, A.; Souri, N. Transient liquid phase bonding of Cu and Al using metallic particles interlayers. *Proc. Inst. Mech. Eng. B J. Eng. Manuf.* **2021**, *235*, 1518−1528.

(31) Lee, K. S.; Kwon, Y.-N. Solid-state bonding between Al and Cu by vacuum hot pressing. *Trans. Nonferrous Met. Soc. China* **2013**, *23*, 341−346.

(32) Wei, Y.; Sun, F.; Tan, S.; Liang, S. Study on microstructure and performance of transient liquid phase bonding of Cu/Al with Al-based interlayers. *Vacuum* **2018**, *154*, 18−24.

(33) Kim, D.; Kim, K.; Kwon, H. Interdiffusion and Intermetallic Compounds at Al/Cu Interfaces in Al-50vol.% Cu Composite Prepared by Solid-State Sintering. *Materials (Basel)* **2021**, *14*, 4307.

(34) Guo, Y.; Liu, G.; Jin, H.; Shi, Z.; Qiao, G. Intermetallic phase formation in diffusion-bonded Cu/Al laminates. *J. Mater. Sci.* **2011**, *46*, 2467−2473.

(35) Ma, H.; Ren, K.; Xiao, X.; Qiu, R.; Shi, H. Growth characterization of intermetallic compounds at the Cu/Al solid state interface. *Mater. Res. Express* **2019**, *6*, No. 106544.

(36) Zhang, J.; Wang, B. H.; Chen, G. H.; Wang, R. M.; Miao, C. H.; Zheng, Z. X.; Tang, W. M. Formation and growth of Cu−Al IMCs and their effect on electrical property of electroplated Cu/Al laminar composites. *Trans. Nonferrous Met. Soc. China* **2016**, *26*, 3283−3291.

(37) Çelik, S.; Ay, I.; Otmanbölük, N. Diffusion Bonding of Pure Copper and Aluminium in Argon Gas Atmosphere. *Pract. Metallogr.* **1997**, *34*, 417−429.

https://doi.org/10.1021/acsomega.3c02838
ACS Omega 2023, 8, 26332−26339